PERGAMON

International Journal of Heat and Mass Transfer 41 (1998) 4251–4257

International Journal of HEAT and MASS TRANSFER

Maximum density effect on laminar water pipe flow solidification

C. W. Tsai, S. J. Yang, G. J. Hwang*

Department of Power Mechanical Engineering, National Tsing Hua University, Hsinchu 30043, Taiwan

Received 21 May 1997; in final form 13 March 1998

Abstract

This paper investigates experimentally and numerically the effect of maximum density on laminar water pipe flow solidification. To visualize the secondary flow patterns and ice morphology experimentally, the water was seeded with a small amount of mercurochrome solution. The numerical analysis employs the large Prandtl number assumption and considers a gradual variation of solid shell in the streamwise direction. The experimental parameters cover the ranges of the dimensionless axial length from 0.008 to 0.32, the inlet water temperature from 5 to 20°C, the wall temperature from −12 to 0°C and the Rayleigh number from 10^4 to 3×10^6. The comparison of the measured and calculated heat transfer rates are in good agreement for wide ranges of operating parameters.

Nomenclature

a tube radius [m]
c specific heat of liquid [J kg^{-1} K^{-1}]
D tube diameter $= 2a$ [m]
e eccentricity of liquid core [m]
g gravitational acceleration [m s^{-2}]
Gr Grashof number $= g\beta_0\,(T_0-T_f)a^3/v^2$ based on tube radius
h heat transfer coefficient [W m^{-2} K^{-1}]
k fluid thermal conductivity [W m^{-1} K^{-1}]
$\dot{m}$ mass flow rate [g s^{-1}]
Pr Prandtl number $= v/\alpha$
q local heat transfer rate [W m^{-2}]
$\bar{q}$ total heat transfer rate [W]
q^* dimensionless heat transfer rate, $q^* = \bar{q}/\pi a^2 w_0\rho_0 c(T_0-T_f)$
r, ϕ cylindrical coordinates [m, rad]
R, ϕ dimensionless cylindrical coordinates, $R = r/ra(z)$
$ra(z)$ peripherally averaged liquid phase radius [m]
Ra Rayleigh number $= Pr\,Gr$
Re Reynolds number $= w_0D/v$
T temperature [°C]
w_0 mean flow velocity at inlet [m s^{-1}]
u, v, w velocity components [m s^{-1}]
U, V, W dimensionless velocity components
z, Z dimensional and dimensionless axial distance, $Z = z/aPr\,Re$.

Greek symbols
α thermal diffusivity [m^2 s^{-1}]
β thermal expansion coefficient [K^{-1}]
δ dimensionless liquid phase radius $= ra(z)/a$
λ superheat ratio $= k_1(T_0-T_f)/k_s(T_f-T_w)$
v kinematic viscosity [m^2 s^{-1}]
θ dimensionless temperature $=(T-T_f)/(T_0-T_f)$
ρ water density [kg m^{-3}]
σ standard deviation of wall temperature [°C].

Subscripts
a average
b bulk
e outlet
f freezing point or fully developed state
l liquid
o inlet
w wall.

1. Introduction

Little work has been carried out on the effect of natural convection on the flow and heat transfer characteristics

* Corresponding author.

0017–9310/98 $19.00
PII: S0017–9310(98)00129–X

during the internal solidification. Usually, those problems in engineering are not examined fully analytically. The main mathematical difficulty comes from the nonlinearity due to the moving of the liquid–solid interface and the natural convection effect. The position of the interface is not known a priori and its location must be determined by the solution itself. In addition, fluids like liquid bismuth, antimony, gallium, tellurium, or water exhibit a maximum density near their freezing points. This property needs a special attention for water, because the maximum density at 4°C frequently encounters in environment (lakes, oceans, melting of icebergs) and in cooling of freezing processes. During the solidification of liquid with a maximum density, the buoyancy complex flow controls the growth of the solid shell.

In the past three decades, both experimental [1–4] and theoretical [1–3, 5] work has been done on the liquid solidification in the thermal entrance region of a horizontal isothermally cooled tube. The magnitude of the Rayleigh number Ra was of the order of 10^6–10^7 in Zerkle and Sunderland [1], 10^5–10^6 in Depew and Zenter [2], $<10^4$ in Hwang and Shue [3], and 10^6 in Mulligan and Jones [4]. All the theoretical researches [1–5] did not consider the effect of natural convection on the solidification. The measured heat transfer rate was 100% higher than the theoretical one [1] without the natural convection. In Depew and Zenter [2], the experimental value was 80% higher. A reasonable agreement was found in [3] for $Ra < 10^4$. Hwang and Tsai [6] investigated numerically the effect of natural convection on the solidification by assuming a circular liquid flow passage. The predicted heat transfer rates agree fairly well with the existing experimental data. In this study, the Rayleigh number, the superheat ratio and the dimensionless superheat ratio are the parameters of the problem.

Although there are many studies on the flow visualization techniques, the mixed convective flow pattern with maximum density effect in internal pipe has not been revealed yet. The difficulty with visualizing the flow pattern may be due to the small buoyancy force $\Delta\rho/\rho \sim 10^{-4}$. Recently, the problem was solved. The visualized secondary flow patterns were clearly exhibited by photographs in Hwang and Tsai [7]. With the maximum density effect, the inlet water temperature T_0 appears as an additional parameter. A detail description on the visualization technique for vortical water flow patterns, ice shell and water–ice interface was reported in Hwang and Tsai [8].

According to the authors' best knowledge, the mixed convection liquid solidification with density inversion effect has not yet been reported systematically. This study makes an attempt to examine theoretically and experimentally the maximum density effect on water flow solidification in a horizontal isothermally cooled pipe. The inlet fully developed water flow with a constant temperature $T_0 > 4$°C is cooled in the pipe with a wall temperature $T_w < 0$°C.

2. Experimental study

The experimental test loop used in this study has been described in detail in Hwang and Tsai [7]. This experimental setup included a constant temperature water reservoir, a constant head tank, a cooling system, and a test section. The constant temperature water reservoir stored distilled water to provide a desired flow rate to the test section. The test section with a cooling length of 81.1 cm was made of copper tube and the jacket was a Plexiglas tube. A Plexiglas light-guided ring was embedded between copper tubes to lighten the cross-section for flow visualization from the outlet. The cross-section was 76 cm from the inlet. A ring type lamp was mounted around the light-guided ring to provide the light source. A series of photographs were taken at this lightened section which had a variation in the water flow rate. In order to achieve the constant wall temperature conditions, three pairs of inlet and outlet coolant tubes individually controlled the coolant flow rate. Each inlet and outlet of the coolant piping had four coolant passages equi-peripherally located around the outer tube of the test section. The adjustment of the coolant flow rate at each passage regulated the wall temperature distribution.

To visualize the secondary flow patterns and ice morphology, the water was seeded with a small amount of mercurochrome solution [7] when the system achieved its steady state condition. Without the help of the color, exhibited by the mercurochrome solution in the water flow, it was hard to see the solid phase and the liquid–solid interface. The mercurochrome solution was diluted with distilled water at a ratio of 30:1 to ensure that the flow pattern was well exhibited and not disturbed. The light emitted from the ring-type lamp illuminated circumferentially the seeded water flow. Photographs were taken using Fuji ISO 400 film, exposure time 0.5 s and an aperture of 3.5.

Before the test, the facility operated at least for 6 h to reach its steady state condition when temperature variations at the inlet and outlet were less than 0.1°C. In some cases, supercooling occurs for wall temperature near -1°C. Under these circumstances, it may take a long time to reach the steady state. To overcome this difficulty, a coolant, with temperature much lower than the desired wall temperature, was supplied to produce the nuclei of ice. After the formation of the nuclei, the temperature was then rapidly adjusted to the desired wall temperature. The operating conditions were set as

(1) The mass flow rate $\dot{m}$ was from 40 g s^{-1} to 1 g s^{-1}. The corresponding dimensionless axial length $Z = 0.5z/\dot{m}(\rho\alpha\pi)$ varied approximately from 0.008 to

0.32; that was long enough to reveal the natural convection inversion process [7]. Following the flow going through the inversion process, the fluid with negative β moves upwards for lower fluid temperature; that is opposite to the fluid with positive β before the process.

(2) The inlet water temperature T_0 was from 5 to 20°C. Due to the combined effect of variations of ΔT, β and ν, the natural convection effect on the laminar flow solidification could be studied in the range of Rayleigh number $10^4 \leqslant Ra \leqslant 3\times10^6$.

(3) The wall temperature T_w was set at $-12 \leqslant T_w \leqslant 0$°C.

3. Theoretical analysis

Consider a laminar mixed convection flow in the thermal entrance region of a circular pipe. The inlet water, with a fully developed velocity and a constant inlet temperature, flows into an isothermally cooled pipe, as depicted in Fig. 1. Ice formation occurs on the pipe wall. Due to the secondary flow induced by natural convection, the thickness of the solid ice shell is not circumferentially uniform. Liquid solidification without maximum density effect was studied previously in pipe flow [6]. The analysis also assumed a circular liquid core. On the contrary, Hwang and Tsai [7] considered the maximum density effect on laminar mixed convection pipe flow without solidification. The present investigation further extends these studies considering liquid solidification with maximum density effect.

The solution to the solidification problem can be treated in three parts: the liquid phase, the solid phase and the liquid–solid interface. For clarity, one can refer the derivation of the governing equations and the associate boundary conditions to Hwang and Tsai [6, 7]. In the analysis, the governing parameters are the inlet water temperature, the Rayleigh number, the superheat ratio and the dimensionless axial length. The inlet water temperature T_0 was from 5 to 20°C. Due to the maximum water density at 4°C, the inlet temperature affects the secondary flow patterns in this temperature range.

The dimensionless heat transfer rate q^* from 0 to Z is

$$q^* = \frac{\bar{q}}{\pi a^2 w_0 \rho_0 c(T_0 - T_f)} = \frac{4}{\pi}\int_0^Z\int_0^\pi -\left.\frac{\partial\theta}{\partial R}\right|_{R=1} \mathrm{d}\phi\,\mathrm{d}z$$

where

$$\bar{q} = 2a\int_0^z\int_0^\pi -k\left.\frac{\partial T}{\partial r}\right|_{r=a} \mathrm{d}\phi\,\mathrm{d}z$$

is the overall heat transfer rate. By considering the overall temperature drop between the inlet and the outlet sections, the dimensionless heat transfer rate q^* can be written readily as $q^* = (T_0 - T_e)/(T_0 - T_f)$.

4. Results and discussion

In this study, a total of 53 experimental runs were conducted to examine the mixed convection effect on the solidification process in the water pipe flow. Of these, 35 were to provide a comparison of q^* with the existing data and the present analytical solution. The remaining 18 were conducted to take photographs of the ice morphology and flow patterns. Data reduction and experimental uncertainty analysis were performed using the same method as that adopted by Hwang and Tsai [7]. The percentage of experimental uncertainty of q^* and Z was calculated as $\delta q^*/q^*$ and $\delta Z/Z$, respectively. Most of the value of $\delta q^*/q^*$ lies within 5% and may reach a maximum value of 7%. For $\delta Z/Z$, the values are less than 2%. All thermophysical properties were evaluated at the film temperature T_r. Conductivity ratio of liquid to solid k_l/k_s is 0.25.

Comparison of the measured Q^* and the existing test data with the present theoretical prediction is shown in Fig. 2. The ranges of Ra, T_0 and λ in Zerkle and Sunderland [1], Depew and Zenter [2] and Hwang and Sheu [3] are also listed in this figure. It is noted that the computed data were obtained by using the mean values of Ra, T_0 and λ in the previous works. The agreement between the experimental data and theoretical calculation is fairly good. In comparison with earlier work [6], the

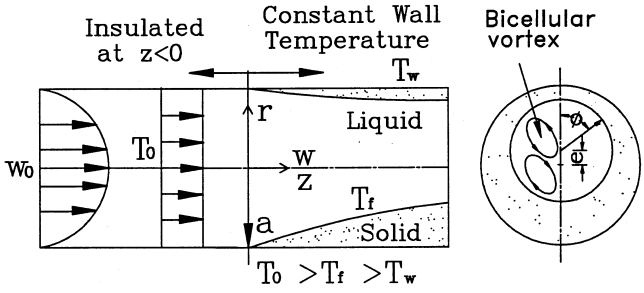

Fig. 1. Physical model and coordinate system.

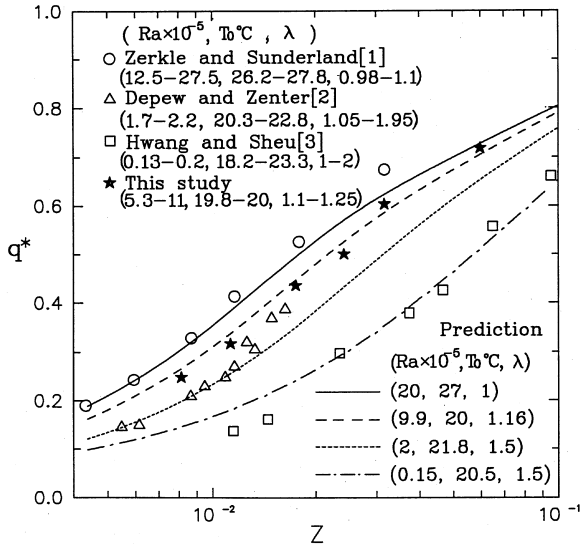

Fig. 2. Comparison of measured q^* and existing test data with theoretical prediction.

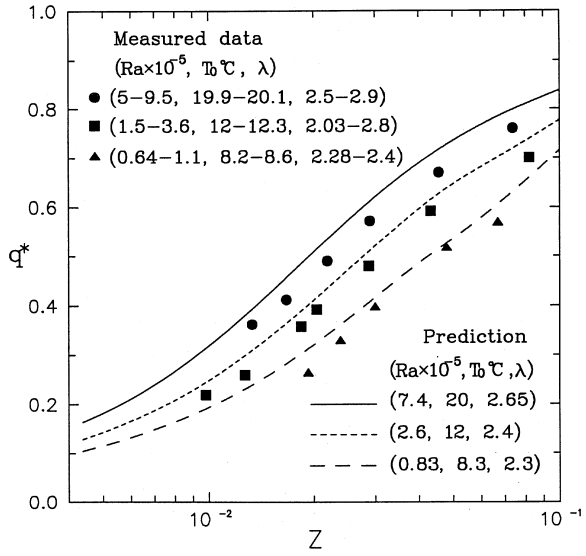

Fig. 3. Comparison of measured q^* with theoretical calculation for $\lambda \approx 2.4$.

accuracy of predicted q^* can be estimated by average error which is defined as

$$\sum_{i=1}^{N}\left(\frac{|q^*_{\exp}-q^*_p|}{q^*_p}\right)\Big/N$$

in which $q^*_{\exp}$, q^*_p and N are the experimental data, predicted value and the number of the experimental run, respectively. The average error of q^* in the previous study [6] for Zerkle and Sunderland [1] is 9%, for Depew and Zenter [2] is 11% and for Hwang and Sheu [3] is 8%, respectively. In this study, the average error of q^* for Zerkle and Sunderland [1] is 6%, for Depew and Zenter [2] is 9% and for Hwang and Sheu [3] is 6%, respectively. The comparison of the measured q^* with the theoretical calculation for $\lambda \approx 2.4$ is plotted in Fig. 3. Three inlet water temperatures (20, 12 and 8°C) were properly controlled to reveal the effect of inlet water temperature on q^*. From this figure, one sees that the agreement between the present prediction of q^* and the measured data is quite satisfactory. For a fixed pipe diameter, the heat transfer rate q^* increases with an increase in the inlet water temperature T_0 and the Rayleigh number.

By controlling the inlet water temperature and the wall temperature and adjusting the water flow rate, a sequential evolution of ice–water interface morphology and flow patterns can be observed. Photographs of ice–water interface morphology and flow patterns as well as the calculated ones for $T_0 \approx 20$°C and $\lambda \approx 2.65$ are presented in Fig. 4. The green color of the mercurochrome solution [7] seems to extend into the ice shell. In order to exhibit clearly the ice–water interface, a hand drawing of the ice–water interface was made on the photograph. In Fig. 4(a), the cooled water flow moved downward along the upper side wall. On the other hand, the flow near the lower bottom wall was decelerated by the opposite buoyancy force. The slow secondary motion near the lower bottom wall caused the deposition of ice in this region. Therefore, the shape of the liquid core passage looks like an ellipse with a longer horizontal axis. As the main flow moved downstream, the secondary counter rotating vortex near the bottom wall developed as shown in Fig. 4(b). These two vortices met at $\phi \approx 90°$. The shape of the flow passage looks like a spindle. The strength of the secondary vortex near the bottom wall increased because of the continuous cooling of the flow. The angular position, where two vortices met, shifted to the upper portion of the flow as shown in Fig. 4(c)–(e). The shape of the flow passage looks like an ellipse with a long vertical axis. Theoretical predictions of streamlines and ice thickness showed qualitative agreement with the experimental results. Since circular shape of flow passage is assumed in this study, the ice–water interface morphology exhibited large discrepancy between experimental and predicted results.

Photographs of flow patterns and ice–water interface morphology are shown in Figs 5 and 6 for $T_0 \approx 12$°C and $T_0 \approx 8$°C, respectively. These two figures show the same trend as presented in Fig. 4. In Fig. 5(e) and Fig. 6(d) and (e), colder water <4°C was transported to the upper part of the flow. The center of the liquid core moved downwards. Since the strength of the secondary motion became weaker at the late stage of solidification process, the deposition of ice was mainly dependent on the solid

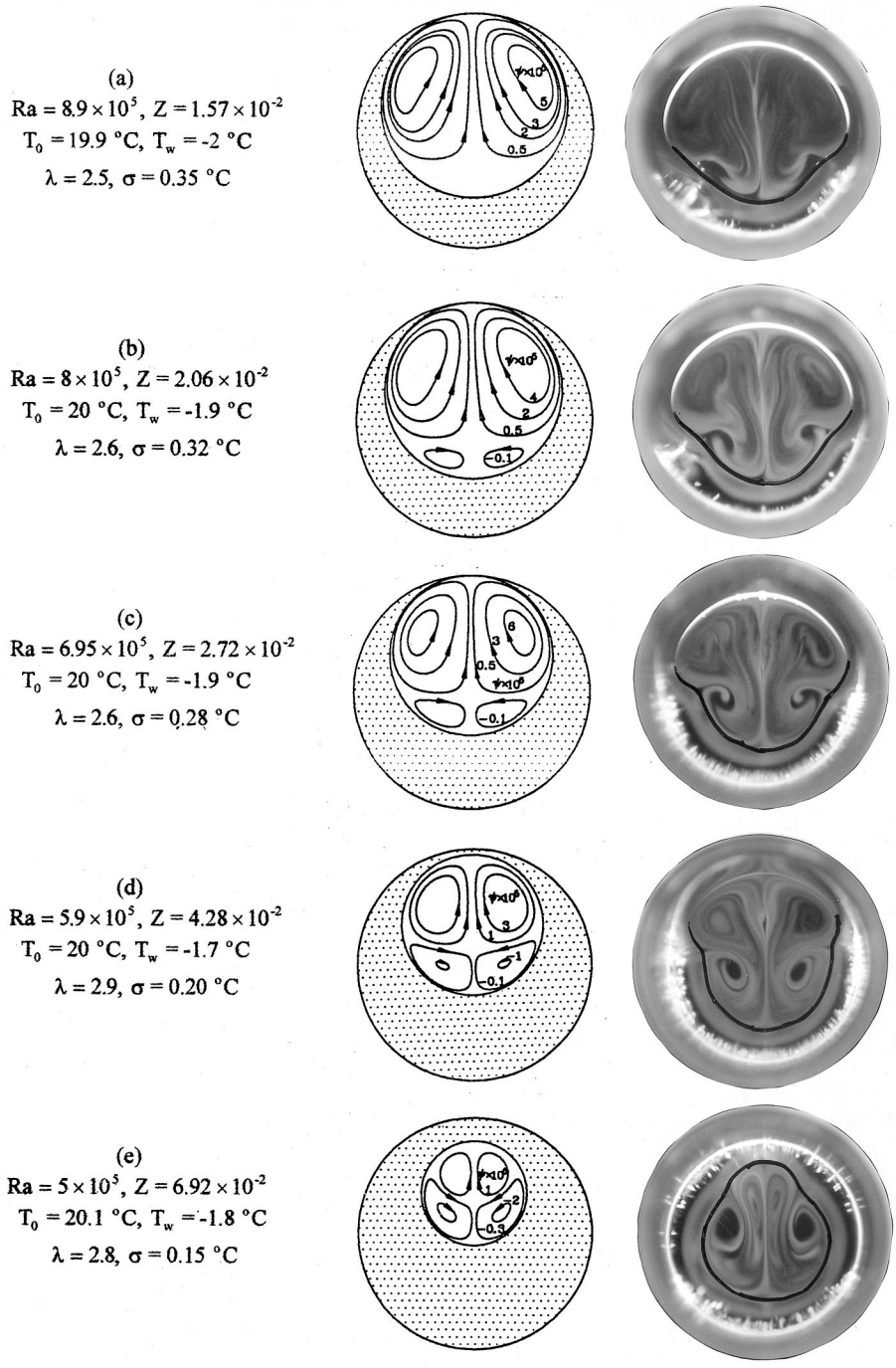

Fig. 4. Photographs of ice morphology and flow patterns for $T_0 \approx 20^\circ C$ and $\lambda \approx 2.65$.

heat conduction. This equalized the solid thickness and the flow passage returned to circular shape.

Comparison of the predicted liquid core radius δ and the dimensionless eccentricity e/a with the measured data are presented in Figs 7 and 8, respectively. The liquid core radius δ is the square root of the ratio of the flow passage area to the pipe cross-sectional area. The ratio of the flow passage area to the pipe cross-sectional area

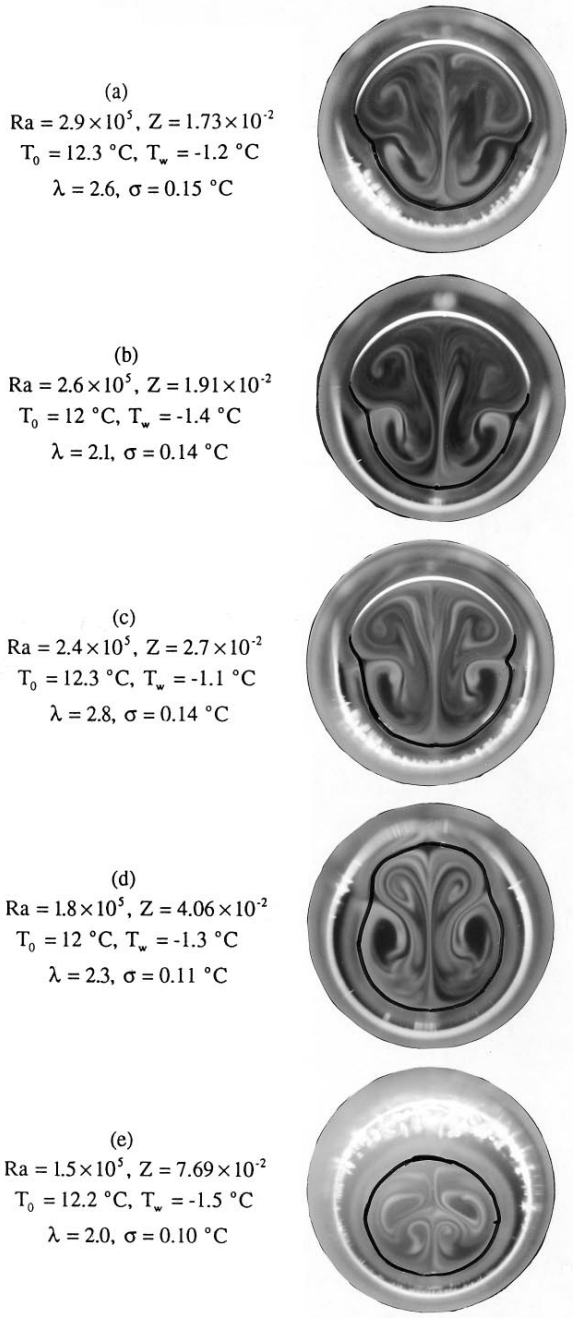

Fig. 5. Photographs of ice morphology and flow patterns for $T_0 \approx 12^{\circ}C$ and $\lambda \approx 2.4$.

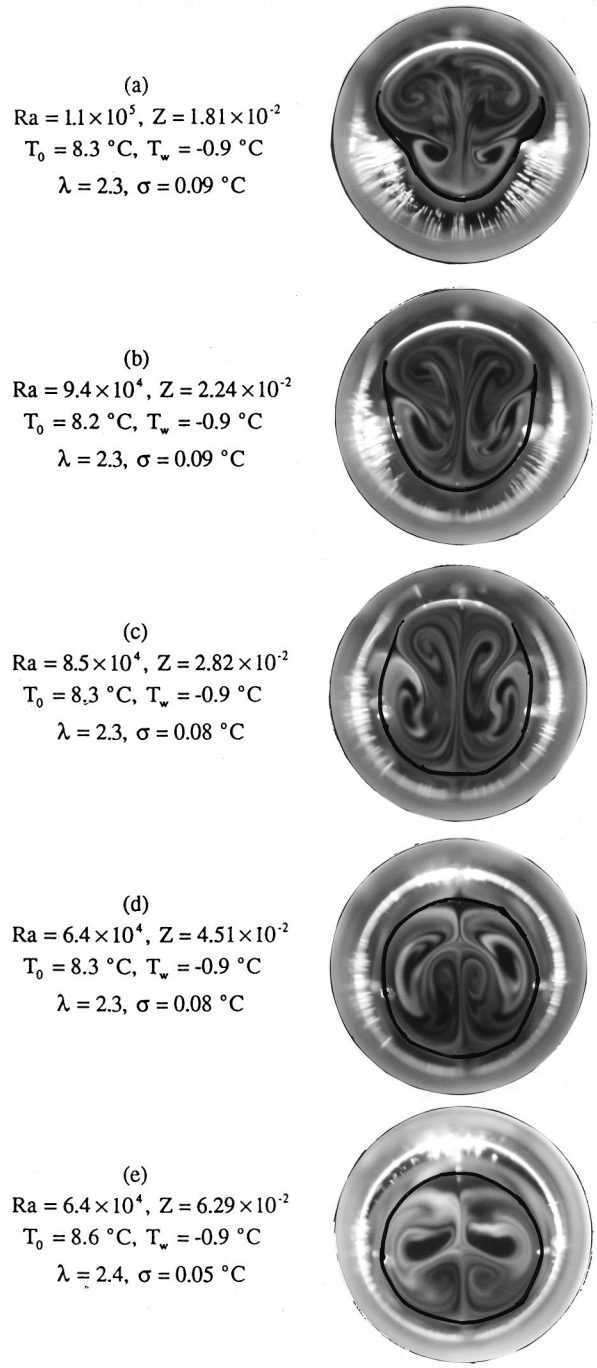

Fig. 6. Photographs of ice morphology and flow patterns for $T_0 \approx 8^{\circ}C$ and $\lambda \approx 2.3$.

of each photograph was measured by manual calculation. The image of each photograph was magnified and placed under tracing paper. The amount of meshes surrounded by flow passage on the tracing paper was thus calculated. The eccentricity e is the difference between the center of the liquid core and the pipe center. The measured and predicted data qualitatively agree with each other for both δ and e/a. It is noted that close consistency between experimental data and prediction were found in the upstream region, while large discrepancies appear in the

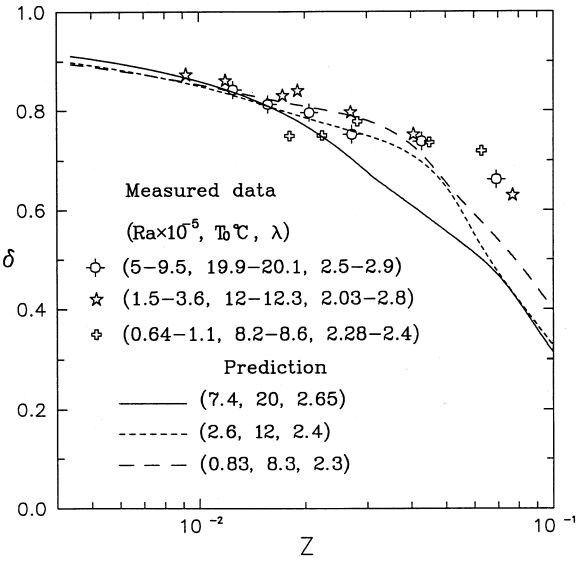

Fig. 7. Comparison of predicted liquid core radius δ with measured data.

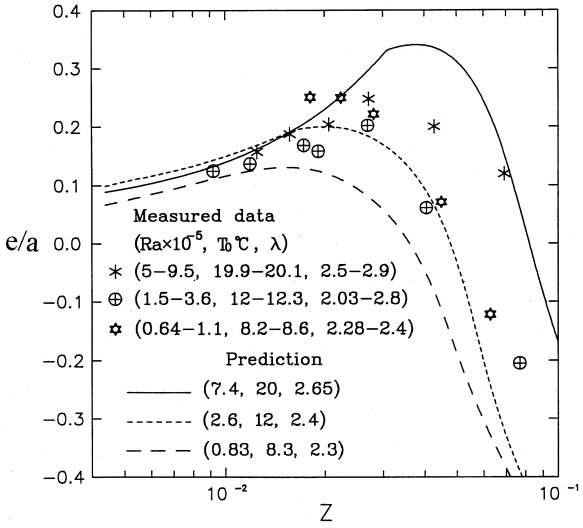

Fig. 8. Comparison of predicted dimensionless eccentricity e/a with measured data.

downstream region. This was due to the assumed circular liquid core and the one dimensional solid heat conduction model of theoretical analysis. These two assumptions deviated from that of the experimental observation in the downstream region.

5. Conclusions

The study of mixed convection effect on laminar water flow solidification in a horizontal isothermally cooled pipe with the maximum density effect has been carried out experimentally and numerically. The parameters are the local Rayleigh number, the inlet water temperature and the superheat ratio. The numerical and experimental results provide a comprehensive understanding of the maximum density effect of water on the solidification process. An analysis of the flow patterns and heat transfer characteristics shows that the maximum density of water affects the solidification process significantly. Conclusions can be made as follows:

(1) The comparison of the calculated and measured heat transfer rates are in good agreement for wide ranges of operating parameters, regardless of the difference between the assumed circular liquid core and the observed ones.
(2) The flow patterns and ice morphology were successfully visualized by injecting a diluted mercurochrome solution in the test section.
(3) With the maximum density effect, the formation of two pairs of counter rotating vortices deforms the shape of liquid core at different locations. The liquid core passage changes its shape from horizontal ellipse, spindle, vertical ellipse and to a circular one at its final stage.

References

[1] R.D. Zerkle, J.E. Sunderland, The effect of liquid solidification in a tube upon laminar flow heat transfer and pressure drop, Journal of Heat Transfer 90 (1968) 183–190.
[2] C.A. Depew, R.C. Zenter, Laminar flow heat transfer and pressure drop with the freezing at the wall, International Journal of Heat and Mass Transfer 12 (1969) 1710–1714.
[3] G.J. Hwang, J.P. Sheu, Liquid solidification in combined hydrodynamic and thermal entrance region of a circular tube, The Canadian Journal of Chemical Engineering 54 (1976) 66–71.
[4] J.C. Mulligan, D.D. Jones, Experiments on heat transfer and pressure drop in a horizontal tube with internal solidification, International Journal of Heat and Mass Transfer 19 (1976) 213–219.
[5] M.N. Özisik, J.C. Mulligan, Transient freezing of liquids in forced flow inside circular tube, Journal of Heat Transfer 91 (1969) 385–390.
[6] G.J. Hwang, C.W. Tsai, Effect of natural convection on laminar pipe flow solidification, International Journal of Heat and Mass Transfer 38 (1995) 2733–2742.
[7] G.J. Hwang, C.W. Tsai, Theoretical and experimental studies of laminar mixed convection in water pipe flow with density inversion effect, International Journal of Heat and Mass Transfer 40 (1997) 2019–2033.
[8] G.J. Hwang, C.W. Tsai, A flow visualization technique for vortical water flow inside a pipe, Proceedings of the 1st Pacific Symposium on Flow Visualization and Image Processing 1 (1997) 174–178.